PROCEEDINGS OF SPIE

SPIEDigitalLibrary.org/conference-proceedings-of-spie

Manufacture and performance of blazed soft x-ray transmission gratings for Arcus and Lynx

Heilmann, Ralf, Bruccoleri, Alexander, Song, Jungki, Levenson, Bethany, Smallshaw, Brian, et al.

Ralf K. Heilmann, Alexander R. Bruccoleri, Jungki Song, Bethany Levenson, Brian Smallshaw, Mallory Whalen, Alan Garner, Sarah Trowbridge Heine, Herman L. Marshall, Matthew T. Cook, James A. Gregory, Renee D. Lambert, Dmitri Shapiro, Douglas J. Young, Eric M. Gullikson, Tomoyuki Nonaka, Akimi Uchida, Manuel A. Quijada, Ed Hertz, Peter Cheimets, Randall K. Smith, Mark L. Schattenburg, "Manufacture and performance of blazed soft x-ray transmission gratings for Arcus and Lynx," Proc. SPIE 11822, Optics for EUV, X-Ray, and Gamma-Ray Astronomy X, 1182215 (23 August 2021); doi: 10.1117/12.2594951

SPIE.

Event: SPIE Optical Engineering + Applications, 2021, San Diego, California, United States

Manufacture and performance of blazed soft x-ray transmission gratings for Arcus and Lynx

Ralf K. Heilmann[a], Alexander R. Bruccoleri[b], Jungki Song[a], Bethany Levenson[b], Brian Smallshaw[b], Mallory Whalen[a], Alan Garner[c], Sarah Trowbridge Heine[c], Herman L. Marshall[c], Matthew T. Cook[d], James A. Gregory[d], Renee D. Lambert[d], Dimitri A. Shapiro[d], Douglas J. Young[d], Eric M. Gullikson[e], Tomoyuki Nonaka[f], Akimi Uchida[f], Manuel A. Quijada[g], Ed Hertz[h], Peter Cheimets[h], Randall K. Smith[h], and Mark L. Schattenburg[a]

[a]Space Nanotechnology Laboratory, MIT Kavli Institute for Astrophysics and Space Research, Massachusetts Institute of Technology, Cambridge, MA 02139, USA
[b]Izentis, LLC, Cambridge, MA 02139, USA
[c]MIT Kavli Institute for Astrophysics and Space Research, Massachusetts Institute of Technology, Cambridge, MA 02139, USA
[d]MIT Lincoln Laboratory, Lexington, MA 02421, USA
[e]Lawrence Berkeley National Laboratory, Berkeley, CA 94720, USA
[f]Samco Inc., Kyoto 612-8443, Japan
[g]NASA Goddard Space Flight Center, Greenbelt, MD 20771, USA
[h]Center for Astrophysics, Harvard-Smithsonian Astrophysical Observatory, Cambridge, MA 02138, USA

ABSTRACT

The soft x-ray band covers the characteristic lines of the highly ionized low-atomic-number elements, providing diagnostics of the warm and hot plasmas in star atmospheres, interstellar dust, galaxy halos and clusters, and the cosmic web. High-resolution spectroscopy in this band is best performed with grating spectrometers. Soft x-ray grating spectroscopy with $R = \lambda/\Delta\lambda > 10^4$ has been demonstrated with critical-angle transmission (CAT) gratings. CAT gratings combine the relaxed alignment and temperature tolerances and the low mass of transmission gratings with high diffraction efficiency blazed in high orders. They are an enabling technology for the proposed Arcus grating explorer and were selected for the Lynx Design Reference Mission grating spectrometer instrument. Both Arcus and Lynx require the manufacture of hundreds to perhaps $\sim$ 2000 large-area CAT gratings. We are moving toward CAT grating volume manufacturing using 200 mm silicon-on-insulator wafers, 4X optical projection lithography tools, deep reactive-ion etching, and KOH polishing. We have, for the first time, produced high-throughput 200 nm-period CAT gratings $\sim$ 50% deeper than previously fabricated. X-ray diffraction efficiency is significantly improved in the $\sim$ 1.25 - 1.75 nm wavelength range, peaking above 40% (sum of blazed orders). A new grating-to-grating alignment technique utilizing cross-support diffraction of visible light is presented, as well as the results of CAT grating emissivity measurements.

Keywords: Arcus, Lynx, critical-angle transmission grating, x-ray spectroscopy, blazed transmission grating, soft x-ray, grating spectrometer, high resolving power

1. INTRODUCTION

The characteristic lines of the highly ionized lighter and most abundant "metals" in the universe lie in the soft x-ray band. High-resolution spectroscopy of these lines in absorption and emission provide invaluable density, temperature and velocity diagnostics for the plasmas that harbor these metals. This knowledge in turn can teach us about cosmic feedback on the scale of galaxy clusters, as well as about baryon dynamics outside and within

Further author information: (Send correspondence to R.K.H.)
E-mail: ralf at space.mit.edu, , URL: http://snl.mit.edu/

Optics for EUV, X-Ray, and Gamma-Ray Astronomy X, edited by Stephen L. O'Dell, Jessica A. Gaskin, Giovanni Pareschi, Proc. of SPIE Vol. 11822, 1182215 · © 2021 SPIE · CCC code: 0277-786X/21/$21 · doi: 10.1117/12.2594951

our own Milky Way. On the scale of solar systems accretion of hot gas also generates soft x-ray spectra with rich plasma diagnostics, informing us about the dynamics of star formation. These and more science themes for soft x-ray spectroscopy are described in more detail elsewhere.[1,2]

High resolving power ($R = \lambda/\Delta\lambda > 1500$) spectroscopy for soft x rays is best achieved using grating-based instruments.[3] Critical-angle transmission (CAT) gratings - developed over the last decade - combine the relaxed alignment and temperature tolerances and the low mass of traditional transmission gratings with high diffraction efficiency based on efficient blazing into high orders.[4–7]

The two primary currently operating x-ray spectroscopy missions[8,9] were launched 22 years ago and lack both the effective area and the resolving power for the required measurements. However, with today's CAT grating technology we can build an instrument on an Explorer-class budget that is much more powerful than what used to require a flagship mission, as the Arcus? soft x-ray grating Explorer mission concept shows. Arcus features four parallel optical channels, each consisting of a co-aligned array of 12 m-focal length silicon pore optic (SPO) mirror modules,[10] developed for the Athena[11] mission. Each mirror array is followed by an array of over one hundred CAT gratings arranged on the surface of a tilted Rowland torus.[12–14] Arcus will have an effective area of at least 200 cm^2 and $R > 2500$ over the 1-3 nm wavelength range, exceeding figures of merit of current spectrographs by factors of at least 5-10.

The 2020 Astrophysics Decadal Review is evaluating four Surveyor-class mission concepts. One of them, the Lynx[15] x-ray observatory, features a retractable grating array for large-area (> 4000 cm^2) high-resolution ($R > 5000$) soft x-ray spectroscopy, covering a fraction of a large x-ray optic. A CAT grating spectrometer made of ~ 2000 large-area gratings[16–18] was selected for the Design Reference Mission described in the Lynx X-ray Observatory Report.[19] As part of this effort we developed a detailed Technology Development Roadmap that can take CAT grating technology from today's state-of-the-art to Technology Readiness Level (TRL) 6 for Lynx by 2024.[20]

Given the large number of gratings required for either Arcus or Lynx we have dedicated significant effort to develop fabrication techniques that support high-volume production of CAT gratings.[21] At the same time we strive to continue to improve grating performance. We have recently succeeded in fabricating several CAT gratings with well over 5 μm in depth, a roughly 45% improvement over previous 4 μm deep gratings.

After a brief overview of the CAT grating principle and grating structural design we describe our fabrication approach and path toward deeper and more efficient gratings. We then discuss recent record x-ray diffraction efficiency results for these deeper gratings. This is followed by grating bar tilt angle measurements from deep-reactive ion etched (DRIE) 200 mm silicon-on-insulator (SOI) wafers. Next we describe an improved grating roll alignment method that uses diffraction from the CAT grating cross-support mesh in transmission, and grating emissivity measurements, before we conclude and summarize.

2. CAT GRATING PRINCIPLE AND STRUCTURAL HIERARCHY

CAT gratings are comprised of ultra-high aspect-ratio, freestanding grating bars with nm-smooth sidewalls.[22] The gratings are inclined such that x rays of wavelength λ impinge on the sidewalls at graze angles θ below the critical angle for total external reflection θ_c (see Fig. 1). The grating equation provides the m^{th} order diffraction angle β_m via

$$\frac{m\lambda}{p} = \sin\theta - \sin\beta_m, \tag{1}$$

with p being the grating period. Diffraction orders near the direction of specular reflection from the sidewalls show increased efficiency (i.e., blazing). The small critical angles for soft x rays (typically on the order of 1-2 degrees) demand high-aspect ratio grating bars in order to intercept all incoming photons. Furthermore, the bars need to be as thin as possible to minimize absorption. The grating period cannot be too large compared to the x-ray wavelength to obtain diffraction orders that can be sorted by order using the energy resolution of Si-based detectors. We initially chose a design with grating period $p = 200$ nm, grating bar depth $d = 4$ micrometers, and bar thickness $b \approx 60$ nm. Such a grating is most efficient when $\tan\theta \approx (p - b)/d$, or $\theta \approx 2$ deg.

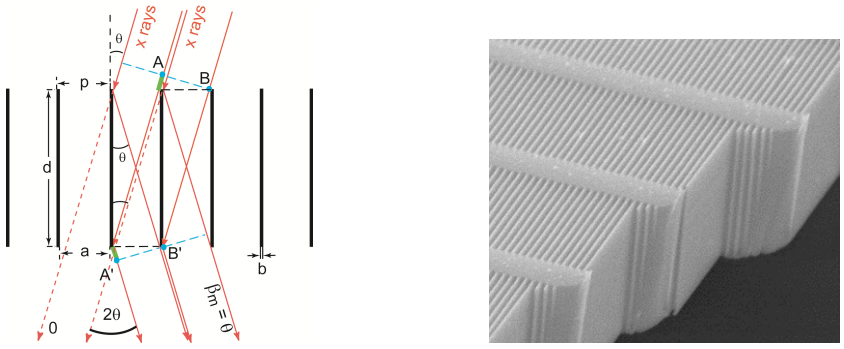

Figure 1. Left: Schematic cross-section through a CAT grating of period p. The m^{th} diffraction order occurs at an angle β_m where the path length difference between AA' and BB' is $m\lambda$. Shown is the case where β_m coincides with the direction of specular reflection from the grating bar sidewalls ($|\beta_m| = |\theta|$), i.e., blazing in the m^{th} order. Right: Scanning electron micrograph of a cleaved CAT grating membrane showing top, cross-section and sidewall views of the 200 nm-period silicon grating bars and their monolithically integrated 5 μm-period cross supports (x rays enter from the top and leave out the bottom).

CAT grating bars are not supported by a membrane, but freestanding. As seen on the right in Fig. 1, the bars are held in place by a monolithically integrated 5 μm-period Level 1 (L1) support mesh. Additional support structures are needed for the few-μm thin grating layer in order to manufacture large enough CAT gratings that can cover large areas on the order of thousands of square centimeters with a reasonable number of gratings. Fig. 2 shows an additional, much thicker and stronger Level 2 (L2) hexagonal support structure on the scale of $\sim$ 1 mm. The photograph on the right shows a so-called silicon grating membrane, etched from an SOI wafer and featuring an additional Level 3 (L3) frame around the edge. This edge is used to bond the membrane to a metal frame that serves as the mechanical interface to a larger machined grating array structure (GAS).

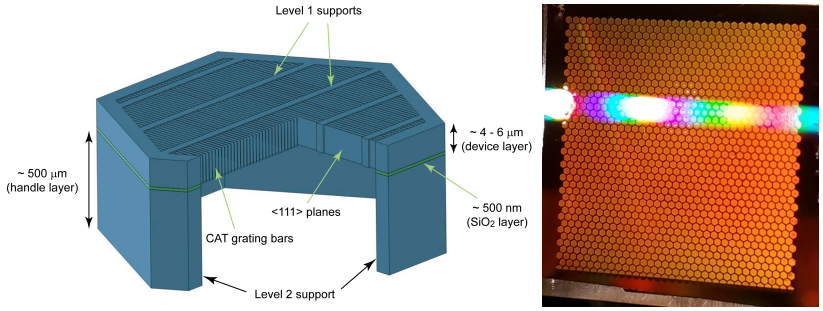

Figure 2. Left: Schematic showing the structural hierarchy of a CAT grating membrane (not to scale). Right: Photograph of an existing 32 x 32 mm^2 CAT grating membrane with back illumination to show the hexagonal L2 mesh, and with visible light diffraction due to the L1 mesh.

3. FABRICATION OF >5 MICROMETER DEEP CAT GRATINGS

We have fabricated numerous CAT gratings with depths around 4 μm, mostly using two separate interference lithography steps on 100-mm SOI wafers for the 200 nm-period CAT grating pattern and the 5 μm-period L1 cross supports.[23,24] The CAT grating lines are patterned parallel to one set of vertical {111} planes in the (110) device (front side) layer. The patterns are then transferred from resist into a thermal oxide layer, which serves as the etch mask for the deep reactive-ion etch through the nominally 4 μm-thick device layer. The buried oxide (BOX) layer serves as the etch stop for both device layer and handle (back side) layer DRIE. After front side DRIE the grating is immersed in KOH solution for a short anisotropic polishing step that reduces the DRIE-produced scalloping on the grating bar sidewalls that are parallel to the device layer {111} planes (see example

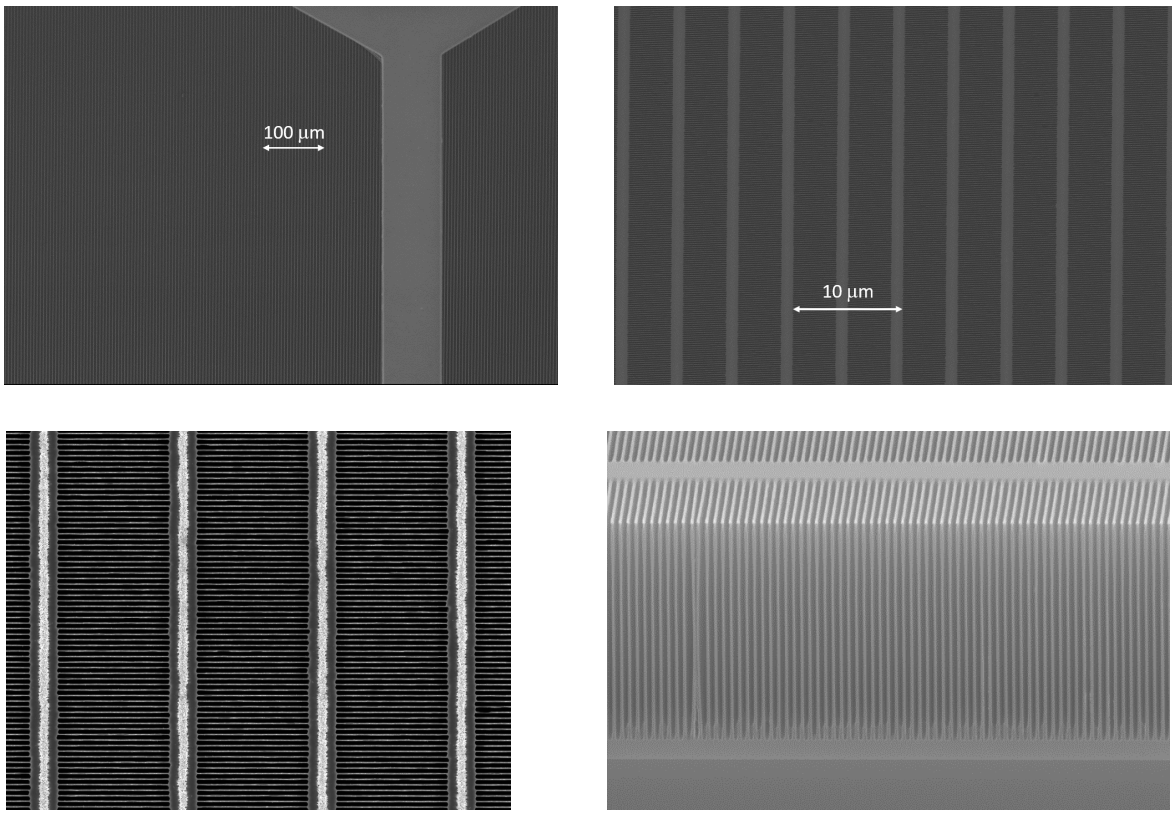

Figure 3. Scanning electron micrographs of deep CAT gratings. Top Left: View of a piece of the back side L2 mesh and the barely visible L1 support mesh. Top Right: Front side view of the L1 mesh and the 200 nm-period CAT grating bars. Bottom Left: Zoomed in view of the CAT grating bars anchored by the 5 μm-period L1 mesh. In this image the remaining L1 oxide mask has not been fully removed yet. Bottom Right: Cleaved cross section of a deep etch (on a SAMCO RIE-800iPB) through a ~ 5.3 μm thick device layer stopping on the BOX layer and after the subsequent KOH polishing step.

images in Fig. 3). The grating is then protected with Protek or evaporated Ti and bonded to a carrier. The back side is covered with thermal oxide and an additional plasma-enhanced chemical vapor deposition (PECVD) oxide layer plus photoresist. We pattern the back side with a 1-mm period hexagonal L2 mesh and DRIE this pattern all the way through to the BOX layer. The open areas of the BOX layer are removed via RIE and vapor HF etch, resulting in freestanding CAT grating bars.

Arcus uses 4 μm deep gratings with 30% duty cycle (b/d) as a baseline. The various etch steps must therefore achieve grating bar aspect ratios on the order of $4000/60 \approx 70$, which is quite challenging. After years of development we now achieve this aspect ratio fairly routinely.

Recently we moved to 4X optical projection lithography with e-beam written photomasks that transfers the CAT grating, L1, and front side L2 patterns into resist in a single step.[21] The exposure field of the MIT Lincoln Laboratory (LL) ASML lithography tool is stepped across full 200-mm SOI wafers, maintaining pattern phase continuity across field boundaries. Using a maskless aligner (MLA) the back side L2 pattern is aligned to the front side L2, and L3 patterns are added that define the edges of each individual grating membrane. We can fit the patterns for 21 Arcus-sized gratings (about 32×32 mm^2 each) on a 200-mm wafer, or we can easily switch to any other L3 custom grating dimensions and layouts with the MLA. However, transferring our 100-mm fabrication process from campus tools onto a different set of tools at LL and MIT.nano for 200-mm wafers required an intense, multi-year effort.

Simulations predict that increasing grating depth from 4 to 6 μm will increase CAT grating diffraction

efficiency significantly and extend the useful bandpass toward shorter wavelengths.[24] This requires the etching of 60 nm-wide grating bars with aspect ratios > 100. Reducing the width from 60 to 40 nm would increase efficiency further.

We were unable to achieve 6 μm deep etches that would result in good-quality and large-area freestanding gratings using older 100 mm and 150 mm DRIE tools available to us in Cambridge. Fortunately, Samco was willing to perform DRIE demonstrations on one of their current-generation 200 mm tools in Japan. After some process development they were able to perform a number of full-wafer etches that reached the BOX layer without excessive notching of the grating bar bottoms. One of the main problems was the variability of the device layer thickness (nominally 6 μm) across the 200 mm SOI wafers on the order of ± 1 μm, which often led either to failure to reach the BOX or unacceptable notching. The acquisition of 200 mm SOIs with much better controlled device layer thickness will be a priority in future efforts.

From the wafers etched by Samco we recently were able to produce over a dozen freestanding gratings in the Arcus format.

The photomask was designed with a 15% duty cycle for the L1 mesh. We did not anticipate that optical proximity effects, stepper illumination, and subsequent pattern transfer steps would result in an increased L1 duty cycle. SEM images on the final gratings show L1 duty cycles in the range of 20-23%. (In earlier grating generations we had fabricated several gratings with duty cycles of 8-15%.) The next photomask iteration will be biased accordingly for a final L1 duty cycle near 15%.

4. CAT GRATING DIFFRACTION EFFICIENCY FOR > 5 MICROMETER DEEP GRATINGS

The first nominally 6 μm deep freestanding CAT grating was tested at the MIT Kavli Institute's (MKI) x-ray polarimetry beamline at B, C, and O-K characteristic lines and showed promising diffraction efficiency and homogeneity across the sample. We subsequently were able to obtain time at beamline 6.3.2 of the Advanced Light Source (ALS) at Lawrence Berkeley National Laboratory shortly before its 3-month shutdown. We hand-carried a plate with six new Arcus-sized CAT gratings (four of 6 μm depth and two of 4 μm depth) to the ALS. Due to Covid restrictions the gratings were mounted in the beamline by ALS personnel, and the measurements were performed remotely.

Due to limited beam time the gratings were measured in various amounts of detail. Most of the time was spent on gratings SEG25 and SEG30, both nominally 6 μm deep. Most of the measurements consisted of sample rocking scans (rotate the grating around an axis parallel to the CAT grating bars at the intersection of the x-ray beam and the grating, thereby varying the x-ray incidence angle onto the grating bar sidewalls), with the slit-covered detector centered on a transmitted diffraction peak. Due to the alignment-insensitive transmission geometry the diffracted orders move so little during rocking scans that the detector can remain stationary. The beam cross section was not measured, but is typically on the order of $\sim 50 \times 250$ μm^2 at the sample position, averaging across many L1 periods. For most of the data the beam was centered inside an L2 hexagon.

We took data at 1.0, 1.25, 1.5, 1.75, and 2.38 nm wavelengths. Similar to the blazed orders that the long readouts for Arcus would cover, we plot the sum of diffraction efficiencies from the blazed orders at a fixed incidence angle in Fig. 4. Compared to previous data from 4 μm deep gratings we see the large (up to 150% relative) gain in diffraction efficiency, especially in the 1.25 to 1.75 nm range. Individual blazed orders showed record absolute efficiencies above 25%, and the maximum sum of orders was found to be above 40% absolute efficiency, also a record for CAT gratings.

Not surprisingly, the deeper gratings achieve their best performance at smaller incidence angles than the shallower gratings (1.5 and 1.66 degrees vs. ~ 1.8 degrees). Use of these gratings would therefore suggest a shift of the readouts towards smaller angles for maximum effective area increase, at a slight cost in average resolving power.[14,16,25]

Initial x-ray data analysis indicates a grating depth of 5.6-5.8 μm and average grating bar width $< b >$ around 60 nm for SEG25, and $d \approx 5.3$-5.6 μm and $< b > \approx 50$ nm for SEG30. These estimates are derived from data taken at a single spot for each grating.

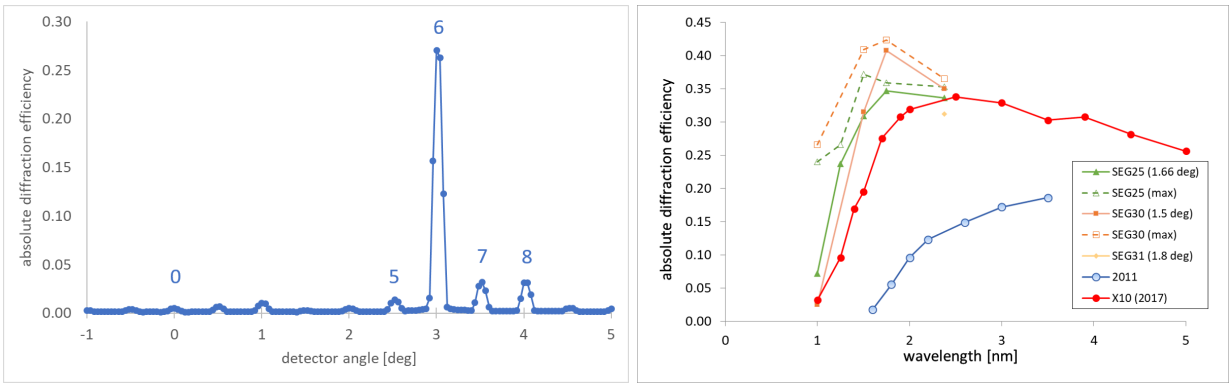

Figure 4. Left: Detector scan from grating SEG25 at 1.75 nm wavelength. X rays are incident at an angle of $\sim 1.66°$. Orders near the angle of specular reflection ($\sim 2 \times 1.66°$) have enhanced diffraction efficiency, in this case, especially, 6^{th} order with an absolute efficiency of 27%. Right: Sum of absolute efficiencies of orders near the blaze angle as a function of wavelength. The solid lines correspond to orders that would be collected by the current Arcus readout design, and the dashed lines add additional neighboring orders with a few percent efficiency. For example, the value of the "SEG25 (1.66 deg)" line at 1.75 nm is the sum of orders 5-9 from the left figure, while the value for the dashed line also adds in the 4^{th} order efficiency. X10 is a 4 μm deep grating fabricated four years ago, and "2011" refers to one of the first x-ray testable CAT gratings measured in 2011. The deeper gratings SEG25 and SEG30 display significantly higher efficiency in the $\sim$ 1-1.75 nm wavelength band.

5. CAT GRATING BAR TILT

As we have described previously,[26,27] the deep etch into the SOI device layer is not perfectly normal to the wafer surface, but the etch angle varies systematically as a function of position on the wafer surface. This results in a variation of the grating bar tilt angle, and therefore also in a variation of the blaze angle. If this variation is too large, a significant fraction of x rays will be diffracted into undesired orders. The variation is a function of etch tool design, etch recipe, wafer size, mask pattern, and whether the etched sample is a chip on a carrier wafer or a full wafer on the wafer chuck.

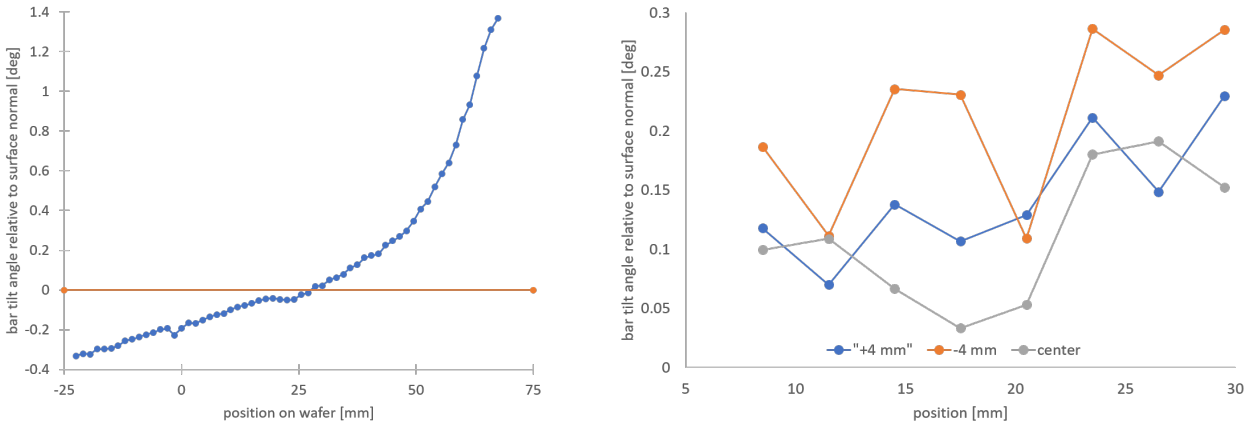

Figure 5. Left: Bar tilt data for part of a 200 mm wafer. The center of the wafer is at position zero. The data was acquired along a straight line ca. 30 mm above the wafer center, perpendicular to the direction of the CAT grating bars. For this wafer the grating pattern extended only about 80 mm from the center, leaving about 15 mm of unpatterned oxide mask at the edge (see Fig. 5 in Ref. 21), which might have lead to charging and bending of field lines during DRIE.[27] More recent wafers are patterned much closer to the edge. Still, most of the area lies within Arcus tolerances. Right: Bar tilt data for grating SEG25, taken along three parallel lines 4 mm away from each other.

Before we can control the bar tilt distribution we must be able to measure it. We recently developed an efficient, precise and accurate bar tilt measurement method using small-angle x-ray scattering (SAXS) and laser reflection.[27] The best results so far are obtained from full wafer etches of 200 mm SOI wafers. If we are just interested in the bar tilt distribution we only need to perform the front side DRIE step and then thin the back side sufficiently (to about 100 μm thickness). Since our SAXS tool can only accommodate small samples we have to break a full 200 mm wafer into chips and measure them separately. The left side of Fig. 5 shows data from a deep etch of a full 200 mm wafer. Over a 75 mm distance the bar tilt only varies by 0.15-0.20 deg per 30 mm, which is about the width of an Arcus grating, and stays within +0.2 and -0.3 deg from the surface normal. This level of variation is within the error budget for Arcus,[14] which means that a large central part of the wafer can be used for the fabrication of flight-quality gratings. The right side of Fig. 5 shows bar tilt data for grating SEG25 as an example of a finished grating, which was deep etched in a full wafer etch, centered about 45 mm from the center of the 200 mm wafer. This grating also has acceptable bar tilt variations for an Arcus grating.

6. GRATING ROLL ALIGNMENT USING L1 DIFFRACTION IN TRANSMISSION

For a large-area grating spectrometer a large number of gratings have to be aligned to each other. Grating tip and tilt can be measured relatively easily from either side using near-normal incidence of a laser beam of any visible wavelength. However, the specular (zeroth order) reflection contains no information about grating roll. For roll we previously demonstrated an alignment method using reflected backdiffraction of a UV laser incident on the CAT grating at a grazing incidence angle of about 30 degrees.[28] While we achieved satisfactory results with this method, it has some drawbacks, namely its sensitivity to grating non-flatness and even slight buckling of the device layer across L2 hexagons. This sensitivity would be much reduced for transmitted orders near the zeroth order transmitted beam, but the angles required to obtain diffraction from a 200 nm-period grating in transmission are large and inaccessible even for UV lasers due to the dimensions of the back side L2 mesh.

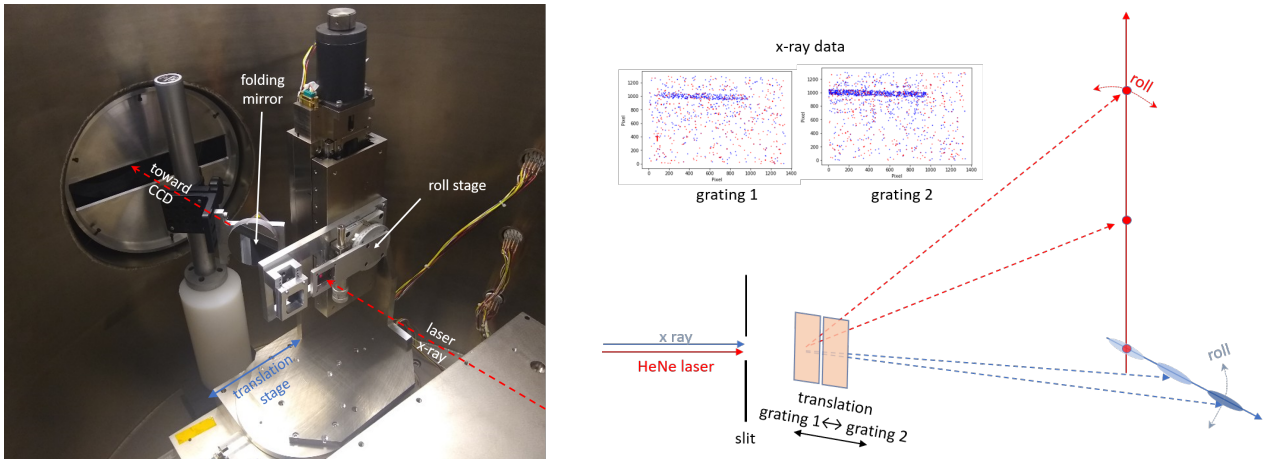

Figure 6. Left: View inside the grating chamber of the MKI polarimetry beamline. Right: Schematic of the proof-of-concept demonstration. The inserts on the upper left show data from the x rays collimated by the slit, diffracted in 2nd order from the CAT grating bars, and recorded by the CCD camera. See text for more details.

The projection lithography photomask contains the CAT grating and L1 patterns at the same fixed angle (90 degrees) to each other for every grating patterned with this mask. Therefore we can utilize a red or green laser near normal incidence and use the diffracted orders from the L1 mesh in transmission as roll alignment references.

To demonstrate this method we used the MKI x-ray polarimetry beamline (see Fig. 6). Two CAT gratings were mounted on a grating translation stage, with one of the gratings mounted to a precision roll stage. The grating normals nominally are parallel to the optical axis of the beamline defined by a red alignment laser coming from the direction of the x-ray source. The grating stage is used to move each grating into and out of the laser beam. The roll variation of this stage between the two grating positions was measured with an autocollimator

to be 0.6 arcmin. A folding mirror just downstream of the gratings projects the transmitted diffraction orders (dispersed vertically) through an open access port out of the vacuum chamber onto a wall about 6 m away. We marked the location of the diffracted beams from the first grating on the wall, translated the second grating into the laser beam, and adjusted its roll angle until its orders overlapped with the marked spots on the wall. We estimated the precision of the overlap to be about 1.25 arcmin in roll. We then removed the folding mirror, closed the grating chamber and pumped down the beamline. A wide horizontal slit (20×1 mm, 0.7 m upstream of the gratings) was used to collimate the x rays 8 m from the source (boron anode, characteristic line at 0.183 keV). For each grating, the 2^{nd} order diffraction (dispersed horizontally) from the CAT grating bars was recorded by the CCD camera, 1.8 m downstream from the gratings. In this orientation grating roll primarily moves the diffracted order vertically up or down. The difference in vertical position of the diffracted x rays was found to correspond to 3.51 ± 0.21 arcmin in roll, resulting in a roll angle difference of ~ 2.9 arcmin after stage error correction.

This number would be good enough for Arcus alignment requirements.[13] At the time of this experiment we could not measure the co-planarity of the two gratings. If they differ from each other enough in yaw and only a single order is used to achieve overlay between gratings via roll adjustments, then roll alignment could suffer from systematic errors. For the alignment of many gratings we are integrating the capability of measuring several L1 diffraction orders in transmission with the grating facet assembly station (GFAS),[12] which can then simultaneously measure and adjust grating pitch, yaw and roll.

7. CAT GRATING EMISSIVITY MEASUREMENTS

In a typical CAT grating spectrometer configuration a large array of gratings is placed just aft of a large focusing mirror array. One side of the array will face the mirrors that are usually held near room temperature, and the other side will face into some kind of shroud or extendable boom with a detector array some 10 meters away, held near -90C. For proper thermal design of the whole payload the thermal properties of the CAT gratings, especially emissivity, need to be known. Instead of trying to model this property for CAT gratings which feature periodic structures on multiple length scales (sub-micron, a few microns, and hundreds of microns) we decided to measure grating reflectance and transmittance and calculate emissivity $\epsilon(T)$ at temperature T from

$$\epsilon(T) = \frac{1 - \int_{\lambda_1}^{\lambda_2} (\rho_d + T_s) P(\lambda, T) d\lambda}{\int_{\lambda_1}^{\lambda_2} P(\lambda, T) d\lambda}, \tag{2}$$

where ρ_d is the total hemispherical reflectance, T_s is the total integrated transmittance, and Planck's function is defined as

$$P(\lambda, T) = \frac{8\pi hc^2}{\lambda^5 (e^{hc/\lambda T k_B} - 1)}. \tag{3}$$

As usual, h is Planck's constant, c is the speed of light in vacuum, and k_B is the Boltzmann constant.

A Bruker FT Spectrometer (IFS125HR) was the instrument of choice to collect data in the 2 to 120 μm spectral range at ambient temperature (300 K). Adequate experimental conditions for measurements in this spectral range were achieved by choosing combinations of the following components: tungsten lamp, Hg arc lamp, or Globar source, Si/CaF2, multilayer Mylar, or Ge/KBr beam splitter and a DTGS (deuterated triglycine sulfate) detector with a KBr window. The reflectance attachment used for these measurements was mounted in the sample compartment of the spectrometer and it consists of a hollow sphere (75 mm diameter) coated with an electro-deposited Lambertian gold coating on the inside. As the left of Fig. 7 shows, the sphere has one beam inlet port, two sample ports and one outlet port allowing the light to reach the detector after the integration. The infrared (IR) beam enters the integrating sphere through the beam inlet port and impinges on the beam-steering mirror which is mounted inside the sphere slightly off center. Depending on the position of the beam-steering mirror, the IR-beam is directed either to the upper or lower sample port. In either case, the angle of incidence for the IR-beam impinging on the sample (or reference) is 13 degrees. In this configuration, the specular and

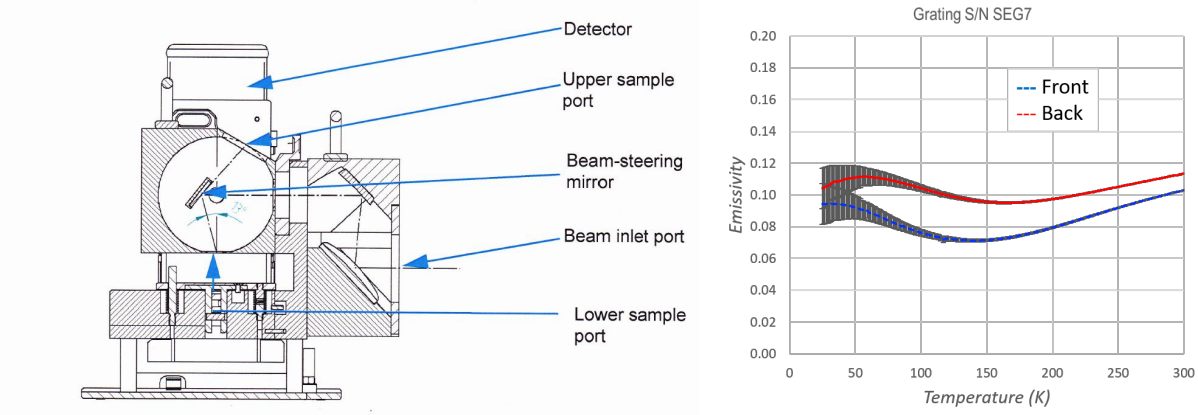

Figure 7. Left: Schematic of the reflectance and transmittance measurements. Right: Calculated emissivity for grating SEG7. The error bars increase for lower temperatures due to the lack of sensitivity of the setup at wavelengths above ~ 100 μm.

the diffusely reflected radiation hit the sphere wall at least once and, therefore, both are included in the flux measurements. In this arrangement no baffles are needed.

We measured the front and back sides of four Arcus-sized gratings fabricated from 100 mm wafers using interference lithography. Only one grating had a front side L2 mesh. Fig. 7 shows emissivity data for grating SEG7 as example, calculated from the measured transmittance and reflectance. Across the four gratings emissivity ranged from 0.08-0.21 for the back and 0.04-0.15 for the front, with the front having lower values at all temperatures for all four samples.

These results are in line with theoretical estimates around 0.1[5] based on simple models, but it is always preferable to have measured values obtained from physical samples.

8. DISCUSSION AND OUTLOOK

CAT grating technology continues to progress. We have identified tools that can achieve close to 6 μm deep etches on 200 nm-period gratings with grating bar aspect ratios close to 110 over most of a 200 mm wafer. These deep etches are made difficult by the ± 1 μm variance in SOI (110) device layer thickness for our current stock of 200 mm SOI wafers. It is imperative that we acquire wafers with better-controlled device layer thickness, ideally on the order of ± 0.2 μm.

The introduction of an aligned front side L2 mesh[21] worked as envisioned and allows longer HF etches to remove mask and buried oxide layers more thoroughly without the danger of device layer delamination. Better oxide removal also appears to reduce device layer buckling to the deep sub-micron level.

We were able to fabricate several high-quality Arcus-size gratings from 200 mm wafers with nominally 6 μm thick device layers. Detailed x-ray synchrotron measurements on gratings SEG25 and SEG30 showed record-high diffraction efficiencies for CAT gratings, especially in the 1.25-1.75 wavelength range. Preliminary x-ray data analysis indicates that the device layer thickness in the areas of measurement was less than 6 μm, and closer to 5.5 μm. Survey scans over these gratings showed good efficiency homogeneity across the whole gratings. Diffraction efficiency can be further improved simply by reducing the L1 mesh bar width from the realized $\sim$ 22% duty cycle to a 15% duty cycle or smaller. CAT gratings with such small duty cycles and 4 μm depths have been made previously and proven to be mechanically robust. The deeper device layers described here are expected to produce even more robust gratings.

Grating bar tilt produced on a demo DRIE tool is acceptable over large areas of 200 mm wafers. No efforts were made to optimize deep etch angles, but we hope to perform experiments in the future to fine-tune etch behavior and to improve bar tilt angle distributions. However, this will to a large degree be contingent on the

acquisition of a dedicated state-of-the-art DRIE tool for this work, since our current main mode of remote work on multi-user tools is not conducive to experimentation that requires many iterations of fine-tuning.

In the past we have produced arrays of two and four aligned CAT gratings and demonstrated x-ray performance that exceeds Arcus resolving power requirements.[12,24] Nevertheless, we continue to work on improvements in our alignment methods, with specific emphasis on improved metrology and automation. Integrating the above roll alignment technique into our GFAS will be a step in the same direction.

In the future we expect to perform Technology Readiness Level (TRL) 5 demonstrations on flight-like arrays of CAT gratings, including environmental testing. The lack of co-aligned high-quality x-ray optics with narrow point-spread function and large geometric illumination area has been somewhat of a roadblock to such demonstrations, but we hope that this situation will improve in the very near future due to technology development in both the US and Europe.

ACKNOWLEDGMENTS

We gratefully acknowledge facility support from Microsystems Technology Labs, the Nanostructures Lab and MIT.nano, all at MIT. A part of this work used resources of the Advanced Light Source, which is a DOE Office of Science User Facility under contract no. DE-AC02-05CH11231. This work made use of the Shared Experimental Facilities at MIT supported in part by the MRSEC Program of the National Science Foundation under award number DMR 1419807. This work was supported by NASA grants 80NSSC19K0335 and 80NSSC20K0780.

REFERENCES

[1] Smith, R. K., *et al.* "The Arcus soft x-ray spectrometer Explorer," *Proc. SPIE* **11444**, 114442C (2020).

[2] Bautz, M. W., "The Lynx x-ray observatory: Science drivers," *Proc. SPIE* **11118**, 111180J (2019).

[3] Heilmann, R. K., Kolodziejczak, J., Bruccoleri, A. R., Gaskin, J. A., and Schattenburg, M. L., "Demonstration of resolving power $\lambda/\Delta\lambda > 10{,}000$ for a space-based x-ray transmission grating spectrometer," *Appl. Opt.* **58**, 1223-1238 (2019).

[4] Heilmann, R. K., Ahn, M., Gullikson, E. M. and Schattenburg, M. L., "Blazed high-efficiency x-ray diffraction via transmission through arrays of nanometer-scale mirrors," *Opt. Express* **16**, 8658-8669 (2008).

[5] Heilmann, R. K. *et al.*, "Critical-angle transmission grating spectrometer for high-resolution soft x-ray spectroscopy on the International X-Ray Observatory," *Proc. SPIE* **7732**, 77321J (2010).

[6] Heilmann, R. K., Ahn, M., Bruccoleri, A., Chang, C.-H., Gullikson, E. M., Mukherjee, P. and Schattenburg, M. L., "Diffraction efficiency of 200 nm period critical-angle transmission gratings in the soft x-ray and extreme ultraviolet wavelength bands," *Appl. Opt.* **50**, 1364-1373 (2011).

[7] Heilmann, R. K., Bruccoleri, A. R., Kolodziejczak, J., Gaskin, J. A., O'Dell, S. L., Bhatia, R., and Schattenburg, M. L., "Critical-angle x-ray transmission grating spectrometer with extended bandpass and resolving power $> 10{,}000$," *Proc. SPIE* **9905**, 99051X (2016).

[8] C. R. Canizares *et al.*, "The Chandra high-energy transmission grating: Design, fabrication, ground calibration, and 5 years in flight," PASP **117**, 1144-1171 (2005).

[9] J. W. den Herder *et al.*, "The reflection grating spectrometer on board XMM-Newton," Astr. & Astroph. **365**, L7-L17 (2001).

[10] Collon, M. J., *et al.*, "Silicon pore optics mirror module production and testing," *Proc. SPIE* **11180**, 1118026 (2019).

[11] http://sci.esa.int/athena/

[12] Heilmann, R. K., *et al.*, "Blazed transmission grating technology development for the Arcus x-ray spectrometer Explorer ," *Proc. SPIE* **10699**, 106996D (2018).

[13] Günther, H. M., Heilmann, R. K., Cheimets, P., and Smith, R. K., "Performance of a double tilted-Rowland-spectrometer on Arcus," *Proc. SPIE* **10397**, 103970P (2017).

[14] Günther, H. M. *et al.*, "Ray-tracing Arcus in Phase A," *Proc. SPIE* **10699**, 106996F (2018).

[15] Gaskin, J. A., *et al.*, "Lynx x-ray observatory: An overview," *J. Astron. Telesc. Instrum. Syst.* **5**, 021001 (2019).

[16] Günther, H. M., and Heilmann, R. K., "Lynx soft x-ray critical-angle transmission grating spectrometer," *J. Astron. Telesc. Instrum. Syst.* **5**, 021003 (2019).

[17] Günther, H. M., and Heilmann, R. K., "Design progress on the Lynx soft x-ray critical-angle transmission grating spectrometer," *Proc. SPIE* **11118**, 111181C (2019).

[18] Günther, H. M., and Heilmann, R. K., "Lynx Grating Spectrometer Design: Optimizing Chirped Transmission Gratings," *Proc. SPIE* **11444**, 1144484 (2020).

[19] https://www.lynxobservatory.com/

[20] https://wwwastro.msfc.nasa.gov/lynx/docs/documents/TechnologyRoadmaps/CAT_TR.pdf

[21] Heilmann, R. K., *et al.*, "Towards volume manufacturing of high-performance soft x-ray critical-angle transmission gratings," *Proc. SPIE* **11444**, 114441H (2020).

[22] Bruccoleri, A. R., Guan, D., Mukherjee, P., Heilmann, R. K., Schattenburg, M. L. and Vargo, S., "Potassium hydroxide polishing of nanoscale deep reactive-ion etched ultra-high aspect ratio gratings," *J. Vac. Sci. Technol. B* **31**, 06FF02 (2013).

[23] Bruccoleri, A. R., Heilmann, R. K., and Schattenburg, M. L., "Fabrication process for 200 nm-pitch polished freestanding ultra-high aspect ratio gratings," *J. Vac. Sci. Technol. B* **34**, 06KD02 (2016).

[24] Heilmann, R. K., *et al.*, "Critical-angle transmission grating technology development for high resolving power soft x-ray spectrometers on Arcus and Lynx," *Proc. SPIE* **10399**, 1039914 (2017).

[25] Günther, H. M., Bautz, M. W., Heilmann, Huenemoerder, D. P., Marshall, M. L., Nowak, M. A., and Schulz, N. S., "Ray-tracing critical-angle transmission gratings for the X-ray Surveyor and Explorer-size missions," *Proc. SPIE* **9905**, 990556 (2016).

[26] Heilmann, R. K., Bruccoleri, A. R., Song, J., and Schattenburg, M. L., "Progress in x-ray critical-angle transmission grating technology development," *Proc. SPIE* **11119**, 1111913 (2019).

[27] Song, J., Heilmann, R. K. and Schattenburg, M. L., "Characterizing profile tilt of nanoscale deep-etched gratings via x-ray diffraction," *J. Vac. Sci. Technol. B* **37**, 062917 (2019).

[28] Song, J., Heilmann, R. K., Bruccoleri, A. R., Hertz, E., and Schattenburg, M. L., "Scanning laser reflection tool for alignment and period measurement of critical-angle transmission gratings," *Proc. SPIE* **10399**, 1039915 (2017).